Journal of Low Temperature Physics (2024) 216:436–449
https://doi.org/10.1007/s10909-024-03178-y

Modification of the Metallic Magnetic Calorimeter Fabrication Process for High Production Yield

J. W. Song[1,2] · S. G. Kim[1] · H. S. Kim[1] · H. J. Kim[2] · M. K. Lee[1]

Received: 29 November 2023 / Accepted: 15 June 2024 / Published online: 9 July 2024

Abstract
We have modified the fabrication processes of metallic magnetic calorimeters (MMCs) to improve production yield. Key modifications include (i) the stress mitigation of the sputtered Nb film by optimizing the Argon deposition gas pressure, (ii) an optimized SiO_X insulator layer fabrication by switching from a lift-off to a wet-etching method and controlling the optimizing the temperature, (iii) the joint electroplating of thick gold structures for persistent current switch leads and a thermalization layer, and (iv) a reduced sputter-deposition time of the Ag:Er sensor material by introducing a new wafer holder. These modifications contribute to increased production yield, reduced fabrication time, and enhanced overall performance. Tests on MMCs fabricated with these modifications demonstrated uniformly improved critical current of the Nb meander coils, enhanced SiO_X insulation properties, strengthened persistent current switch systems, and reduced probability of Ag:Er oxidation. These modified MMC detectors also functioned well in tests for alpha spectrometry measurements, demonstrating good performance.

Keywords Metallic magnetic calorimeter · Low-temperature detector · Critical current · Persistent current switch

1 Introduction

MMCs employing paramagnetic sensor materials such as Ag:Er and Au:Er are designed to measure the energy of particles with high resolution at low temperatures. The energy is determined by precisely measuring the change in magnetization of paramagnetic alloys caused by the heat generated as an incident particle is

✉ M. K. Lee
minkyu@kriss.re.kr

[1] Korea Research Institute of Standards and Science (KRISS), Daejeon 34113, Republic of Korea

[2] Physics Department, Kyungpook National University (KNU), Daegu 41566, Republic of Korea

absorbed by the absorber. To measure the signal from the change in magnetization, a superconducting quantum interference device (SQUID) readout is employed [1].

MMCs have shown excellent performance in the field of nuclear metrology. This extends beyond conventional spectroscopic methods such as alpha-, beta-, and gamma-ray spectroscopy to include novel Q-spectroscopy to measure the characteristic total decay energy of a radioactive nuclide [2–4]. MMC-based spectroscopy offers unprecedented energy resolution, enabling clearer energy separation of closely spaced lines that conventional spectroscopy cannot discern. Additionally, it exhibits excellent energy sensitivity and linearity across a wide energy range, from sub-keV to MeV, making MMCs an ideal tool for precise measurements of the wide spectral range of beta-emitting decay and electron capture [5, 6]. One electron capture experiment, the MetroMMC project organized by various national metrology institutes, has utilized MMCs in radionuclide metrology to improve activity measurements and provide precise nuclear data [6]. In addition, MMC detectors have been widely employed in large-scale experiments such as on neutrinoless double beta decay and dark matter, where their unique advantages are essential [7–9]. Notably, most of these large-scale experiments are currently being scaled up. The advanced molybdenum-based rare process experiment (AMoRE), an ongoing neutrinoless double beta decay experiment, proposes to use several hundred MMC sensors for an upcoming 100 kg experiment with the ^{100}Mo isotope [8]. Process streamlining and optimization are therefore essential to meet the demands of the experimental schedule.

The previously developed fabrication process of MMCs using Au:^{168}Er sensor material consists of several steps, as shown in Table 1 [10–12].

We selected MMCs fabricated by this process through various tests to meet specific requirements necessary for operation. These specifications include a critical current (I_c) of the Nb meander-shaped coils of at least 150 mA, a defect-free SiO_x layer acting as an insulator between the Nb meander coils and the Au:^{168}Er magnetic sensor material, and a robust persistent current switch acting as a switch to inject persistent current in the Nb coils. However, during our testing, we found that only some of the essential requirements were met due to various problems. The I_c of the

Table 1 MMC fabrication process developed in 2013

#	Layer	Method	Description	Thickness
1	Nb	DC sputtering + dry-etching	Meander-shaped pickup coil	400 nm
2	NbO_x	Anodizing	Insulation	40–60 nm
3	SiO_x	PECVD + lift-off	Insulation	150 nm
4	SiO_x	PECVD + lift-off	Insulation	150 nm
5	Ti/AuPd	E-beam evaporator + lift-off	AuPd resistor	10/50 nm
6	Au	E-beam evaporator + lift-off	Persistent current switch leads	800 nm
7	Au:^{168}Er	DC sputtering + lift-off	Paramagnetic sensor	3 µm
8	Au	DC sputtering	Seed layer	100 nm
9	Au	Electroplating + lift-off	Thermalization	4 µm
10	Au	DC sputtering	Seed layer	100 nm
11	Au	Electroplating + lift-off	Stem	5 µm

meander coils is often less than the desired value due to the stress of the deposited Nb film [13]. In the insulating SiO_X layer, defects can arise from micro-pinholes that form during deposition, and the persistent current switch leads can be damaged by electrostatic discharge in weak points created by differences in material height. To address these problems, we modified and optimized various fabrication steps. In addition, streamlining and merging certain fabrication steps allows for a shorter total production time. Further details can be found in the fabrication details section.

2 Fabrication Details

2.1 Stress Mitigation in Nb Film for Improving Superconducting Meander Coil Performance

Operation of an MMC involves injecting a persistent current into two closed superconducting meander-shaped coils. This current generates an external magnetic field, which magnetizes the paramagnetic Au:Er sensor material. Additionally, it serves as a pickup coil to detect signals induced by changes in the magnetization of the Au:Er material resulting from energy absorption. In the current work, a 400 nm thick Nb layer is etched into a meander shape with 100 turns. The meander pickup coils each have a linewidth of 5 μm, a pitch of 10 μm, and a length of 1 mm. Each of the two meanders is 1 mm x 1 mm in size and configured as a first-order gradient type [11].

The Nb meanders fabricated on a 3-inch wafer were characterized at low temperature. Their transition temperatures were nearly the same around 9.1 K, but I_c exhibited a wide range of values, spanning from 20 to 200 mA at 4.2 K. Since, the meander coils had similar transition temperatures but varying I_c, we can reasonably suspect that microcracks were likely to be present in the ~20 cm long Nb lines forming the coils. The presence of microcracks reduces the effective cross-sectional area of the Nb planar line, where the supercurrent flows. The primary cause of defects like these microcracks is believed to be stress in the Nb film deposited on Si wafer [14]. When the etching process creates the meandering pattern, the relaxation of preexisting stress can exert forces on the Nb layer, potentially leading to the formation of defects. We controlled the deposition conditions to make a 400 nm thick Nb film with as much neutral stress as possible.

Figure 1 shows the stress data of Nb films deposited at a deposition rate of 0.4 nm/s on Si wafers using a DC magnetron sputtering system under current modes of 1.1 A with various Ar gas pressures, and the substrate temperature is maintained at 10 °C using active cooling with an antifreeze solution. The stresses in the Nb films were determined by comparing the heights before and after deposition, measured at the wafer scale with a surface profiler. Although the measurement accuracy may be lower, data accumulated over several years indicate that the stress in Nb films deposited at approximately 3 mTorr is nearly neutral. Each Nb meander coil was made using an inductively coupled plasma reactive ion etching (ICP-RIE) process after patterning a positive photoresist (PR) layer. The meander coils were structured by dry-etching at a process pressure of 30 mTorr with mixture gases of SF_6 100 sccm and Ar 50 sccm. The etch rate was 5–6 nm/s at RF power 500 W.

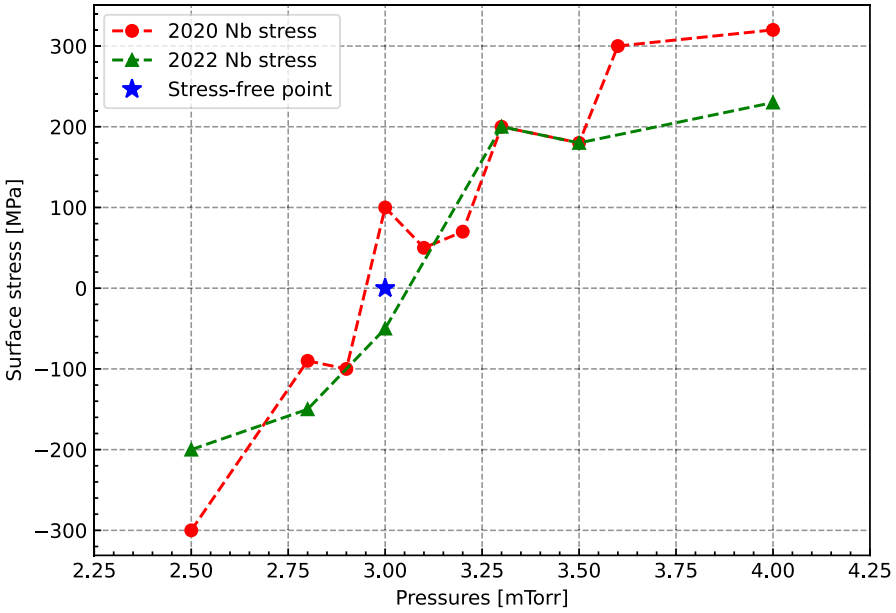

Fig. 1 Stress data for a 400 nm Nb deposition on a Si wafer with 400 µm thickness using DC sputtering at varying gas pressure. Negative and positive values indicate compressive and tensile stress, respectively. The data were measured in the years 2020 and 2022 using a surface profiler. The stress exhibits a neutral characteristic at an Ar pressure of around 3.0 mTorr, marked by the blue star

Tests for electrical properties were conducted on meander-shaped coils manufactured from dry-etched Nb film, including Nb film with a stress level of about −400 MPa (stress-induced sample) and nearly stress-free Nb film with stress levels between −50 and 50 MPa. The resistance of the meander coils was around 23–19 kΩ at room temperature. I_c measurements were carried out with the four-probe method in liquid helium at 4.2 K. The bypass line of the Nb patterns was cut by dicing. The current was gradually increased by 10 mA increments, and the current at the point, where voltage occurred was determined as I_c.

The I_c measurement results are shown in Fig. 2. Sets of randomly selected chips from different wafers were characterized for both datasets. Stress-induced chips were obtained from six stress-induced wafers, and stress-free chips were obtained from two stress-free wafers. The I_c values for stress-induced chips were broadly distributed between 30 mA and 180 mA, as shown in Fig. 2. However, except for one chip, all stress-free chips had I_c values above 150 mA, which is sufficient for MMC detector operation. In most cases, the stress-free chips exhibited I_c values above 200 mA, exceeding the range of the current supply equipment. Stress significantly impacts the I_c of the meander coils, as shown in the histogram. When a mechanical shock is applied to the stress-free meander coils, such as when dicing close to a meander coil, I_c tended to decrease to about 100 mA. Based on these measurements and observations, we can strongly infer

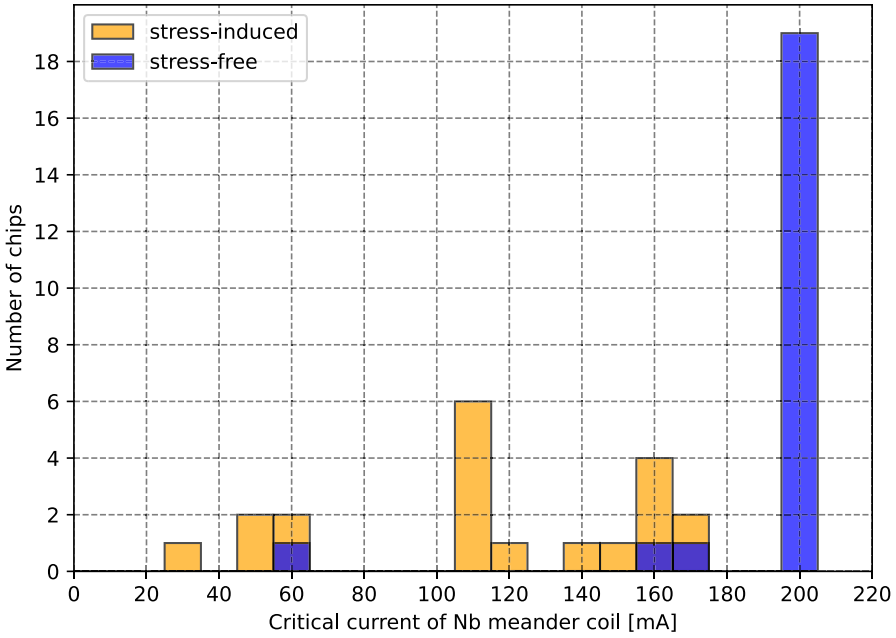

Fig. 2 Histograms of I_c for chips with stress-induced and stress-free meander-shaped coils. The stress-induced data are measured from chips made on wafers with a compressive stress of around −400 MPa, while the stress-free data are measured from chips made on wafers with nearly neutral stress levels ranging from −50 to 50 MPa

that mechanical shock leads to microcracks that decrease the effective cross-sectional area of the Nb meander coils, where the supercurrent flows [14].

2.2 Enhancing the Quality of the SiO_X Insulation Layer by Controlling Deposition Temperature

The SiO_X layer has a dual function, serving as electrical insulation between the Nb meander coils and the paramagnetic sensor material and providing physical protection for the Nb meander coils. To achieve these functions, the SiO_X layer must be free from defects like pinholes. In the previous MMC manufacturing processes, the SiO_X film was deposited using plasma-enhanced chemical vapor deposition (PECVD) after covering electrical Nb pads with a negative PR layer. Then, the unnecessary SiO_X films on the PR were removed by the lift-off process. However, after deposition, we encountered issues with PR hardening. It took 2–3 days to completely lift-off SiO_X in N-Methyl-2-pyrrolidone (NMP) solution at 80 °C. We even had to apply ultrasonic cleaner to assist the lift-off process. To address the PR hardening issue, we attempted deposition at lower temperatures (around 100 °C). However, this low-temperature process can generate defect sites in the SiO_X layer that could cause leakage current. In an attempt to prevent this, we conducted the

deposition of SiO_X in two separate steps, each with a thickness of 150 nm, instead of depositing 300 nm in one step. After finishing the first deposition, the substrate was rotated by 90° before the second deposition to avoid pinhole formation [12]. This approach, though, did not completely resolve all the issues and required the use of ultrasonic cleaners for complete lift-off, thereby increasing the complexity of the process. This, in turn, increased the probability of microcracks in the Nb meander structure.

To address the above issue, we changed from a lift-off process to a buffered oxide etch (BOE) wet-etching method. This method, commonly employed in semiconductor manufacturing, involves using a solution of NH_4F and HF acid to directly etch the SiO_X layer. This solution selectively etches SiO_X much more effectively than NbO_X or Nb [15]. This method allows the deposition of the SiO_X layer directly on the Nb meander pattern without needing PR treatment before the PECVD work. By overcoming the temperature limitations, a more uniform and dense SiO_X layer can be deposited at higher temperatures, effectively reducing the possibility of defects such as pinholes and thus allowing for SiO_X deposition up to 300 nm in a single step. However, the higher deposition temperature may introduce additional compressive stress to the Nb layer, decreasing I_C. Hence, determining the optimum SiO_X deposition conditions is crucial for maintaining the electrical properties of the Nb planar coil and enhancing the protective functions of the SiO_X layer. These optimum conditions were achieved here at 200 °C and a process pressure of 380 mTorr with mixture gases of N_2O 100 sccm and SiH_4 30 sccm. The deposition rate was 1 nm/s at RF power 18 W. BOE wet-etching with a 6:1 solution exhibited an etching rate of 5 nm/s at room temperature.

After the full fabrication process, the resistance of the improved SiO_X layer between the meander coils and the thermalization layer on the paramagnetic sensor was measured at room temperature. For the measurement, a total of 60 chips were randomly selected, with 30 chips chosen from each of two wafers. Out of these 60 chips, 50 operated successfully. Among them, 46 chips exhibited a resistance of over 1 MΩ at room temperature, while the remaining four chips showed a resistance of over 100 kΩ at room temperature. The selective wet-etching method has enabled us to substantially reduce the total fabrication time and increase production yield by avoiding damage to the device elements during prolonged lift-off procedures with ultrasonic cleaners.

2.3 Micrometer-Thick Au Structure Deposition on the Persistent Current Switch System Leads by Joint Electroplating

Our MMCs adopt a gold structure as the leads of the AuPd resistor in the persistent current switch system. Here, 800 nm thick leads were deposited with an electron beam (e-beam) evaporator to overcome the height difference of the structures.

Figure 3a and b depicts scanning electron microscope (SEM) images of the persistent current switches of the MMCs. The AuPd film is deposited on the SiO_X, covering the bypass line of the meander coil. The heat generated by applying a current to the AuPd resistor serves as a current switch that changes the

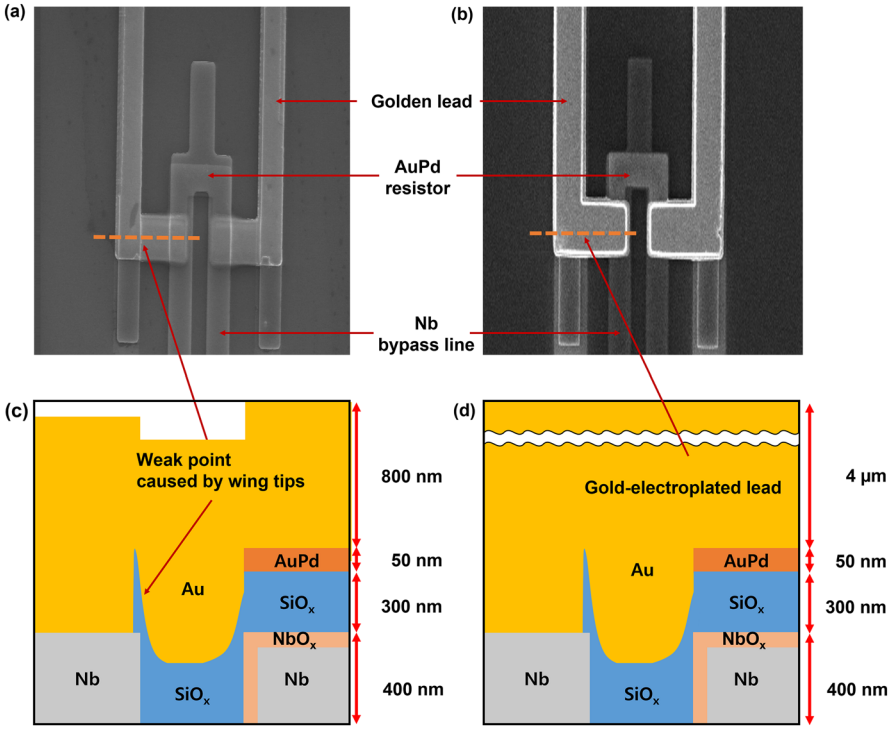

Fig. 3 Persistent current switch system of the MMCs. **a** and **b** SEM images of persistent current switches fabricated using e-beam evaporation and electroplating, respectively. **c** and **d** Cross-sectional schematic view of the area indicated by the orange dashed line in (**a**) and (**b**), respectively. The discernible steps in (**a**) are not present in (**b**), indicating a uniform connection

flow of supercurrent in a moment from the bypass line to the meander coil to inject persistent current [16]. Figure 3c illustrates a schematic cross-sectional view along the dashed line in Fig. 3a of the golden switch leads fabricated using e-beam evaporation. If SiO_X does not drop cleanly in the patterning by lift-off, there is the potential for wing tips to remain on the Nb. As a result, structural defects may occur in the gold leads, leading to increased electrical resistance and making it susceptible to static electricity as a weak point.

To overcome this, a higher thickness of gold deposition is required. For this purpose, the process for the gold leads was merged with the subsequent gold electroplating process for the thermalization layer, which also requires a thick gold layer. To merge these two processes, a new seed layer for electroplating was introduced, which was also used for electroplating the stems. This seed layer was deposited using DC sputtering with a thickness of 100 nm and patterned by lift-off process. The seed layer shown in Fig. 4 represents a segment of the gold seed layer utilized to supply current during electroplating. After patterning a negative PR, the selective area is exposed to an alkaline-based electroplating solution. The patterned PR should not dissolve in the solution during electroplating.

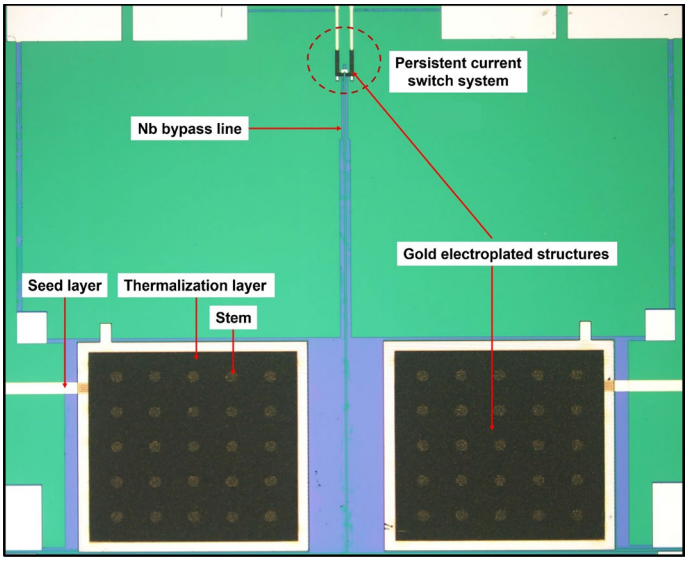

Fig. 4 Microscopy image of an MMC chip showing the seed layer and electroplated parts. The seed layer is connected to the chips in wafer and diced out in the final process. The thermalization layer on the Ag:Er sensor material is jointly electroplated with the leads in persistent current switch system at a thickness of 3 µm

For this, additional steps in the PR process are necessary to ensure the chemical resistance of the PR against the electroplating solution: UV exposure and baking for hardening, and another round of UV exposure for further hardening. This hardening process showed that PR did not dissolve in solution during electroplating. Simultaneous electroplating of leads and thermalization is conducted at a DC current density of 0.3 A/dm^2, a deposition rate of 2 nm/s, and a temperature of 50 °C, achieving a deposition thickness of 4 µm.

In Fig. 3b and d, the persistent current switch after the electroplating process exhibits a uniformly thick gold layer. This region seamlessly connects the Nb and AuPd with no discernible steps and has no weak points in terms of wing tips. Not only were the structural problems in the leads significantly reduced visibly, but also the resistances between the persistent current switch leads were measured much more uniformly on chips across the wafer. The resistances of the persistent current switch were measured to be around 16–18 Ω at 4.2 K. Using the method of selective area electroplating, we were able to produce µm-thick gold layer structures quickly and easily. After electroplating, the PR is dissolved in a chemical solution, eliminating the need for a problematic lift-off process to remove the thick and dense electroplated gold layer from the previous process [12].

Consistent operation conditions for the persistent current switch are crucial for practical use. A single square current pulse ranging in height from 7 to

12 mA was selected to operate the persistent current switch to inject currents of 200 mA or more in the MMC meander. When a current pulse with a height of 100 mA was applied to the AuPd resistor, the center of the AuPd resistor burned out, but the gold leads remained robust in most of the chips.

2.4 Reduction in Sensor Material Deposition Time by Introducing a New Wafer Holder

The deposition process for magnetic sensor material is an essential step in MMC fabrication. This process demands uniformity on the wafer scale, free from contamination by foreign materials, and protection against oxidation of Er. To minimize contamination, the DC sputtering system is typically operated under ultra-high vacuum conditions (base pressure $< 10^{-8}$ Torr). However, because of the deposition of film with a thickness of several μm, the temperature of the wafer inevitably increases during deposition, which can lead to problems such as PR hardening, film contamination with impurities from the PR, and segregation of Er on the film surface [17]. In the previously developed fabrication process, Au:^{168}Er was deposited at a deposition rate of 1 nm/s with 3.0 mTorr Ar gas pressure, taking over 50 min to reach a thickness of 3 μm without excessive heating [12].

Figure 5 is a photograph of the backside of a newly designed holder to enhance wafer cooling. The new wafer holder features a doughnut-shaped structure with metallic ledge encircling the through-hole to support the wafer. Between the circular ledge segment, plate springs made of thin special steel are installed. A clamp with a metal line spring as shown in Fig. 5b pushes the wafer sideways to gently hold it. These heat-resistant elastic plate springs push the wafer upward to the flat substrate of the sputtering equipment, which is cooled with circulating water to maintain a temperature of 10 °C, ensuring close contact of the entire area of the wafer. By using

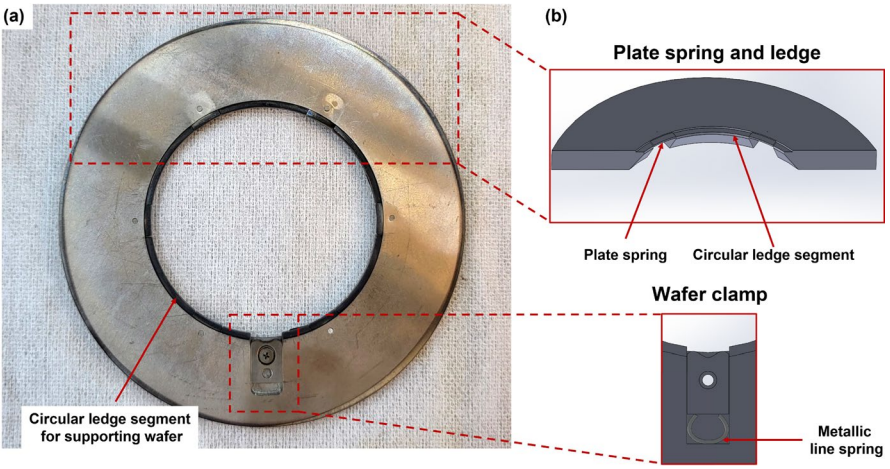

Fig. 5 Photograph and schematics of the new wafer holder. **a** Photo image of the holder, and **b** design of the holder components

the newly designed wafer holder, heat generated from the wafer flows much more efficiently toward the cooling substrate, allowing for the rapid deposition of sensor materials with μm thicknesses without overheating.

For the deposition of the sensor material in the improved process, we used newly synthesized Ag:^{168}Er alloys instead of Au:^{168}Er with concentrations of several hundred ppm. To eliminate potential magnetic impurities and foreign particle generation during DC sputtering, we installed a 2-inch Ag:^{168}Er target in the sputtering gun, securing it with copper centering and bolts instead of stainless steel [18]. The deposition of a 3 μm thick Ag:^{168}Er film was completed in about 16 min, deposited at a deposition rate of 3.1 nm/s with 3.0 mTorr Ar gas pressure and substrate temperature 10 °C. This represents a reduction in the sensor film deposition time by about three times compared to the previous fabrication process, which reduces the risk of Er oxidation during sputtering. Without delay, a 100 nm thick layer of gold was then immediately deposited to prevent potential oxidation on the surface of the Ag:Er film. Using the new wafer holder, we tested MMC chips fabricated by fast deposition of Ag:^{168}Er with an Er concentration of 1000 ppm.

Figure 6 displays the pulse signal heights corresponding to injected current in the Ag:^{168}Er MMC meander coil. A ^{238}Pu source, emitting α-particles with 5.5 MeV energy, was used for measurements at 50 mK. Under the mentioned optimal conditions of the switch, the meander coil injects persistent currents up to 200 mA. Figure 6 exhibits that the pulse height consistently increased as the injected current increased until 150 mA, beyond which it increased more slowly. An energy resolution (E/dE) of 2000 at 5.5 MeV with Gaussian fitting was achieved using a persistent current of 130 mA at 50 mK.

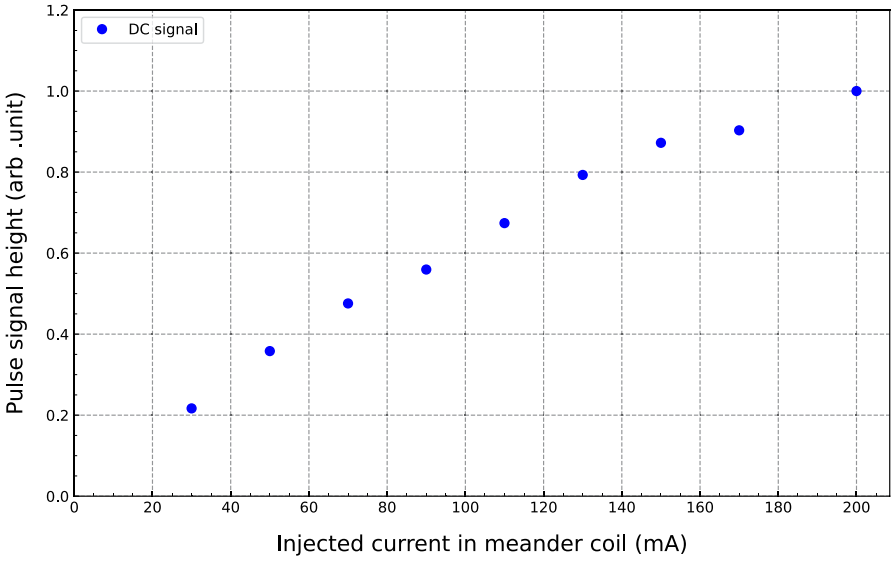

Fig. 6 Relation between injected current and pulse signal height. The signal height was measured with various injected currents in the meander coil. This graph shows that the signal output increases as the current applied to the meander coil increases

Table 2 Modified fabrication process developed in 2021

#	Layer	Method	Description	Modification	Thickness
1	Nb	DC sputtering + dry-etching	Meander-shaped pickup coil	Controlling film stress	400 nm
2	NbO_X	Anodizing	Insulation	–	40–60 nm
3	SiO_X	PECVD + BOE wet-etching	Insulation	Changing lift-off to BOE wet-etching and controlling operation temperature	300 nm
4	Ti/AuPd	E-beam evaporator + lift-off	AuPd resistor	–	10 / 50 nm
5	Ag:^{168}Er/Au	DC sputtering + lift-off	Paramagnetic sensor and protection against Ag:Er oxidation	Using Ag:^{168}Er for sensor material and introducing a new holder	3 µm / 100 nm
6	Au	DC sputtering + lift-off	Seed layer	Introducing a new mask design	100 nm
7	Au	Electroplating	Persistent current switch leads and thermalization	Joint electroplating of persistent current switch leads and thermalization layer and changing lift-off to selective electroplating	4 µm
8	Au	Electroplating	Stem	Changing lift-off to selective electroplating	5 µm

2.5 Modified Fabrication Process

The modified fabrication process developed in this work demonstrates good performance in terms of the I_c of the Nb planar coil, SiO_x insulation layer, and persistent current switches. These good properties are maintained despite stacking multiple layers through an eight-step fabrication process in wafer scale, resulting in obtaining MMCs that meet the specifications required for final use. The modified processes both improve the MMC production yield and considerably simplify the production process, supporting faster manufacturing. The improved process is shown in Table 2.

3 Conclusion

The modified fabrication processes for MMCs have successfully increased production yield, reduced the total fabrication time, and improved the performance of the key elements. The stress mitigation in Nb film by controlling deposition conditions results in a uniformly improved high critical current of the Nb meander coil, exceeding 150 mA across a 3-inch wafer. Changing from lift-off to wet-etching enables the control of the deposition temperature for the SiO_x insulation layer, resulting in a more uniform and less defective structure. In addition, SiO_x wing tips created during the lift-off process can potentially cause weak points in the structural steps, but this does not occur during the BOE wet-etching process. The leads of the persistent current switch were electroplated (4 μm of gold) to enhance both structural robustness and resistance to electric shock-induced burning. Furthermore, the joint electroplating together with the thermalization structures simplified the fabrication process. Additionally, the introduction of a new wafer holder significantly decreases the deposition time for the 3 μm thick Ag:Er sensor material, which reduces the possibility of contamination by trace impurity gases and Er oxidation. These improvements are expected to contribute to the production of reliable MMCs for applications in precision measurement, such as radionuclide metrology and large-scale experiments.

Acknowledgements We would like to thank Dr. Wonsik Yoon at NASA Goddard Space Flight Center for fruitful discussions about writing the paper. We are also grateful to the Center for Underground Physics group of the Institute for Basic Science (IBS), particularly Dr. Jungho So and Dr. Hyelim Kim, for their valuable support and insightful discussions.

Author Contributions J.W. Song conducted the overall experiments and experimental design of this paper. H.S. Kim contributed significantly to the measurements for Fig. 1 in this paper. S.G. Kim contributed to the creation of the electroplating for 2.3 in this paper. M.K. Lee and H.J. Kim contributed to the overall guidance of the experiment.

Data Availability No datasets were generated or analyzed during the current study.

Declarations

Conflict of interest The authors declare no Conflict of interest.

References

1. A. Fleischmann, C. Enss, G. Seidel, *Metallic magnetic calorimeters* (Springer, Berlin, 2005), pp.151–216
2. W. Yoon, C. Kang, S. Kim, G. Kim, H. Lee, M. Lee, J. Lee, J. So, Y. Kim, Development of a high resolution alpha spectrometer using a magnetic calorimeter. Nuclear Instr. Methods Phys. Res. Sect. A: Accel. Spectr. Detect. Assoc. Equip. **784**, 143–146 (2015)
3. S. Friedrich, G.-B. Kim, D. Lee, J.A. Hall, R. Cantor, A. Voyles, R. Hummatov, S. Boyd, Ultra-high resolution magnetic microcalorimeter gamma-ray detectors for non-destructive assay of uranium and plutonium. J. Nuclear Mater. Manag. **49**(3), 114–122 (2021)
4. M. Rodrigues, M. Loidl, S. Pierre, Determination of absolute Np L x-ray emission intensities from 241Am decay using a metallic magnetic calorimeter. Metrologia **60**(2), 025005 (2023)
5. M. Loidl, J. Beyer, L. Bockhorn, J. Bonaparte, C. Enss, S. Kempf, K. Kossert, R. Mariam, O. Nähle, M. Paulsen et al., Precision measurements of beta spectra using metallic magnetic calorimeters within the European metrology research project metrobeta. J. Low Temp. Phys. **199**, 451–460 (2020)
6. P.-O. Ranitzsch, D. Arnold, J. Beyer, L. Bockhorn, J. Bonaparte, C. Enss, K. Kossert, S. Kempf, M. Loidl, R. Mariam et al., MetroMMC: electron-capture spectrometry with cryogenic calorimeters for science and technology. J. Low Temp. Phys. **199**(1–2), 441–450 (2020)
7. B. Mauri, M. Loidl, C. Nones, M. Rodrigues, M. Vivier, First tests of Li_2WO_4 bolometric detectors using MMC sensors for the detection of CEνNS. J. Low Temp. Phys. **211**, 1–7 (2022)
8. S. Kim et al., Searching for Neutrinoless double beta decay with the AMoRE experiments. Il nuovo cimento C **46**(1), 1–9 (2023)
9. B. von Krosigk, K. Eitel, C. Enss, T. Ferber, L. Gastaldo, F. Kahlhoefer, S. Kempf, M. Klute, S. Lindemann, M. Schumann et al., Delight: a direct search experiment for light dark matter with superfluid helium. SciPost Phys. Proc. **12**, 016 (2023)
10. W. Yoon, Y. Jang, G. Kim, H. Lee, J. Lee, M. Lee, Y. Kim, Development of Meander-shaped metallic magnetic calorimeters. Progress Supercond. **14**(2), 102–105 (2012)
11. W. Yoon, G. Kim, H. Lee, J. Lee, J. Lee, Y. Jang, S. Lee, M. Lee, Y. Kim, Fabrication of metallic magnetic calorimeter for radionuclide analysis. J. Low Temp. Phys. **176**, 644–649 (2014)
12. W. Yoon, Magnetic calorimeters for high resolution spectroscopies. PhD thesis, University of Science and Technology, Daejeon, (2014)
13. T. Imamura, T. Shiota, S. Hasuo, Fabrication of high quality Nb/AlO/sub x/-Al/Nb Josephson junctions. I. Sputtered Nb films for junction electrodes. IEEE Trans. Appl. Supercond. **2**(1), 1–14 (1992)
14. S. Zou, R. Bai, G.A. Hernandez, V. Gupta, Y. Cao, J.A. Sellers, C.D. Ellis, D.B. Tuckerman, M.C. Hamilton, Influence of fatigue and bending strain on critical currents of niobium superconducting flexible cables containing Ti and Cu interfacial layers. IEEE Trans. Appl. Supercond. **27**(4), 1–5 (2016)
15. M.V.P. Altoé, A. Banerjee, C. Berk, A. Hajr, A. Schwartzberg, C. Song, M. Alghadeer, S. Aloni, M.J. Elowson, J.M. Kreikebaum et al., Localization and mitigation of loss in niobium superconducting circuits. PRX Quantum **3**(2), 020312 (2022)
16. S. Kim, J. Jeon, I. Kim, H. Kim, S. Kim, D. Kwon, M. Lee, H. Lee, Y. Kim, Critical temperature switch development for metallic magnetic calorimeters. Supercond. Sci. Technol. **32**(5), 054005 (2019)

17. A. Raizman, J. Suss, D. Seidman, D. Shaltiel, V. Zevin, EPR studies of the near-surface layer in a dilute gold-erbium alloy. Phys. Rev. Lett. **46**(2), 141 (1981)
18. J. Song, Y. Cho, H. kim, M. Lee, Synthesis and characterization of an Ag:Er alloy for metallic magnetic calorimeters. to be published, (2024)